Monthly Notices of the ROYAL ASTRONOMICAL SOCIETY

MNRAS **508,** 5354–5361 (2021) https://doi.org/10.1093/mnras/stab2936
Advance Access publication 2021 October 13

Polarization properties of FRB 20201124A from detections with the Effelsberg 100-m radio telescope

G. H. Hilmarsson ,[1]★ L. G. Spitler,[1] R. A. Main[1] and D. Z. Li[2]

[1]*Max-Planck-Institut für Radioastronomie, Auf dem Hügel 69, D-53121 Bonn, Germany*
[2]*Cahill Center for Astronomy and Astrophysics, California Institute of Technology, MC 249-17, Pasadena, CA 91125, USA*

Accepted 2021 October 4. Received 2021 October 1; in original form 2021 July 27

ABSTRACT

The repeating fast radio burst (FRB) source, FRB 20201124A, was found to be highly active in 2021 March and April. We observed the source with the Effelsberg 100-m radio telescope at 1.36 GHz on 2021 April 9 and detected 20 bursts. A downward drift in frequency over time is clearly seen from the majority of bursts in our sample. A structure-maximizing dispersion measure (DM) search on the multicomponent bursts in our sample yields a DM of 411.6 ± 0.6 pc cm^{-3}. We find that the rotation measure (RM) of the bursts varies around their weighted mean value of -601 rad m^{-2} with a standard deviation of 11.1 rad m^{-2}. This RM magnitude is 10 times larger than the expected Galactic contribution along this line of sight (LoS). We estimate an LoS magnetic field strength of 4–6 μG, assuming that the entire host galaxy DM contributes to the RM. Further polarization measurements will help determine FRB 20201124A's RM stability. The bursts are highly linearly polarized, with some showing signs of circular polarization, the first for a repeating FRB. Their polarization position angles (PAs) are flat across the burst envelopes and vary between bursts. We argue that the varying polarization fractions and PAs of FRB 20201124A are similar to known magnetospheric emission from pulsars, while the observed circular polarization, combined with the RM variability, is hard to explain with Faraday conversion. The high linear polarization fractions, flat PAs, and downward drift from FRB 20201124A bursts are similar to previous repeating sources, while the observed circular polarization is a newly seen behaviour among repeaters.

Key words: methods: observational – techniques: polarimetric.

1 INTRODUCTION

Fast radio bursts (FRBs) are short-duration radio transients of extragalactic origin. From the roughly 600 FRBs detected so far,[1] repeating bursts have been detected from 24 FRB sources (Spitler et al. 2016; CHIME/FRB Collaboration 2019, 2021b).

High levels of activity from a repeating FRB source discovered by CHIME, FRB 20201124A,[2] were announced in 2021 March (CHIME/FRB Collaboration 2021a). Active follow-up ensued, where the Australian Square Kilometer Array Pathfinder (ASKAP), the Karl. G. Jansky Very Large Array (VLA), the upgraded Giant Metrewave Radio Telescope (uGMRT), and the European VLBI network localized the source to ∼arcsecond precision (Day et al. 2021; Fong et al. 2021; Law et al. 2021; Marcote et al. 2021; Wharton et al. 2021b). Attempts to detect bursts at higher radio frequencies have yet to be successful (Pearlman et al. 2021; Spitler & Hilmarsson 2021).

The distance to the host galaxy of FRB 20201124A was determined from spectroscopic follow-up observations, which found a redshift of $z = 0.098 \pm 0.002$ (luminosity distance of 453 Mpc) (Day et al. 2021; Kilpatrick et al. 2021). Persistent radio emission in the host galaxy was detected by the uGMRT and the VLA (Ricci et al. 2021; Wharton et al. 2021a). However, Ravi et al. (2021) find that the spatial extent and luminosity of the persistent radio source (PRS) associated with FRB 20201124A are consistent with star formation activity, and place an upper bound on a compact PRS of 3×10^{28} erg s^{-1} Hz^{-1}.

Well-studied repeating FRBs, such as FRB 20121102A and FRB 20180916B, can provide interesting comparison to the properties of FRB 20201124A. The rotation measure (RM) of FRB 20121102A is extremely large, highly variable over time, and consistent with a decade-old supernova remnant (SNR) (Michilli et al. 2018; Hilmarsson et al. 2021). FRB 20180916B's RM is orders of magnitude lower than that of FRB 20121102A, consistent with a several hundred year old SNR (Marcote et al. 2020). Bursts from both FRB 20121102A and FRB 20180916B are highly linearly polarized, with flat polarization angles across the bursts, and exhibit a downward drift in the burst frequency structure (CHIME/FRB Collaboration 2019; Hessels et al. 2019; Chawla et al. 2020). Additionally, a periodicity in activity phases has been found for both FRB 20121102A and FRB 20180916B of 160 d (Rajwade et al. 2020; Cruces et al. 2021) and 16 d (CHIME/FRB Collaboration 2020), respectively.

★ E-mail: henning@mpifr-bonn.mpg.de
[1]https://www.wis-tns.org/
[2]chime-frb.ca/repeaters

Here, we report on our observations of FRB 20201124A with the Effelsberg 100-m radio telescope in Germany. In Section 2, we detail our observations and data reduction. Section 3 provides our results on the properties of FRB 20201124A. In Section 4, we discuss the implications of our results and compare them to other repeating FRB sources. Finally, in Section 5, we summarize our findings.

2 OBSERVATIONS AND DATA PROCESSING

Observations of FRB 20201124A were carried out using the centre pixel of the P217mm seven-beam receiver on the Effelsberg 100-m radio telescope on 2021 April 9 starting at 17:46:10 UTC and lasting 4 h. For the source coordinates (J2000), we used the initial interferometric localization from the ASKAP-CRAFT collaboration: RA = $05^{h}08^{m}03\overset{s}{.}7$ and Dec. = $+26^{d}03^{m}39\overset{s}{.}8$ (Day et al. 2021). Search mode data were recorded with the Pulsar Fast Fourier Transform Spectrometer backend (Barr et al. 2013) at a centre frequency of 1360 MHz and a bandwidth of 300 MHz. The search mode data were total intensity filterbank format with 512 × 0.59 MHz channels and a time resolution of 54.6 μs. The data were recorded natively as 32-bit floats and converted to 8-bit unsigned integers prior to searching. Prior to our observations of FRB 20201124A, we performed a 3-min scan of a 1-Hz noise diode and a 5-min scan of a test pulsar, B0355+54.

The data were searched for single pulses using `HEIMDALL`,[3] `Presto`[4] (Ransom 2011), and `TransientX`[5] from dedispersed time series between 350 and 450 pc cm^{-3} for boxcar widths up to 30 ms, down to a signal-to-noise (S/N) threshold of 7. At this threshold, we are sensitive to bursts down to a fluence of 0.14 × $(W_{\rm ms})^{1/2}$ Jy ms, where $W_{\rm ms}$ is the burst width in milliseconds. For `Presto` and `TransientX`, a DM step of 1 pc cm^{-3} was chosen, while `HEIMDALL` determined its own steps based on pulse broadening induced by the DM step size. `HEIMDALL` missed one of the weaker bursts in our sample, `Presto` missed a strong burst due to it being in a segment of data flagged as radio frequency interference in the `rfifind` mask, and `TransientX` detected all the bursts in our sample.

Voltage data with 1.56 ns time resolution and two polarizations was recorded simultaneously with the search mode data. Around each burst detected in the single pulse search, a 20-s-long segment of data was saved. Coherently dedispersed `PSRCHIVE`[6] (Hotan, van Straten & Manchester 2004) archives containing bursts with full Stokes information were created from the baseband data using `DSPSR`[7] (van Straten & Bailes 2011) and were used to perform all our analysis. The archives were polarization calibrated with a 3-min scan of a 1-Hz noise diode performed prior to our observations using `PSRCHIVE`'s `pac`. We validated our polarization calibration by reconstructing the polarization profile of our test pulsar, B0355+54, as it is in the EPN data base of pulsar profiles,[8] as well as obtaining the same RM (79 rad m^{-2}) as is listed in the ATNF pulsar catalogue[9] (Manchester et al. 2005).

We opted for a structure-maximizing method of determining DMs instead of S/N maximizing due to the latter leading to overlapping sub-components and displaying a broader range of apparent DMs (Hessels et al. 2019). DMs were determined using `DM_phase`[10] (Seymour, Michilli & Pleunis 2019), which performs a Fourier transform on the time series of each frequency channel over a range of trial DMs and then integrates over the emission frequency to produce a coherence spectrum. Fourier frequencies that have similar phase angles will sum to a greater amplitude. This method works better for bursts with sub-components, as the coherent sum will be even greater.

The RMs were determined with RM synthesis (Burn 1966; Brentjens & de Bruyn 2005) using `rmsynth1d` and `rmclean1d` in the RM-TOOLS package[11] (Purcell et al. 2020) for 1000 trial RMs from −2500 to 2500 rad m^{-2}. The RMs are obtained by reconstructing the Faraday dispersion function (FDF) through a Fourier transform of the Stokes Q and U parameters. The width of the FDF peaks rescaled by their maximum S/N represents the 1σ RM uncertainties. We compared our RMs to results obtained with `PSRCHIVE`'s `rmfit` and a Bayesian Lomb–Scargle periodogram RM search method, `RMcalc`[12] (Porayko et al. 2019), and saw consistent values across methods.

3 BURST PROPERTIES AND ANALYSIS

We have detected 20 bursts from FRB 20201124A during our observations. The properties of the bursts are listed in Table 1. We fit a Gaussian, and multiple Gaussians in the case of multiple components, to the profiles of each burst and sub-burst. The burst widths are determined from the full width at half-maximum between the left and rightmost Gaussians. The flux density and fluence are then determined from the widths and receiver parameters using the radiometer equation. The dynamic spectra, intensity and polarization profiles, and polarization position angles (PAs) are shown in Fig. 1. The dynamic spectra in Fig. 1 show clear signs of scintillation that are investigated in Main et al. (2021).

3.1 Periodicity and burst rate

Using a Lomb–Scargle, periodogram we search for periodicities in our sample. We detect no periodicity in burst arrival times from the minimum time difference between bursts in our sample up to the full 4 h of our observation. This is not surprising given the periodicities of FRB 20121102A and FRB 20180916B of 10s/100s days, and no short-time-scale periodicity ($P < 1$ s) has been determined for any repeating FRB (e.g. Pastor-Marazuela et al. 2020; Cruces et al. 2021).

The average burst rate during our observing window is $5.0^{+1.4}_{-1.1}$ bursts h^{-1} above a fluence of 0.14 × $(W_{\rm ms})^{1/2}$ Jy ms for an S/N threshold of 7. We estimate a Weibull distribution clustering parameter of $k = 0.7 \pm 0.1$ using the full sample. If bursts 10 and 11, separated by 30 ms, are consolidated into a single event, we obtain $k = 0.9 \pm 0.2$. A clustering parameter of $k = 1$ reduces a Weibull distribution to a Poissonian one. Therefore, the arrival times of FRB 20201124A during this observation are consistent with a Poisson distribution when bursts separated by $\lesssim$100 ms are excluded, as has also been seen in FRB 20121102A (Cruces et al. 2021).

[3] sourceforge.net/projects/heimdall-astro
[4] github.com/scottransom/presto
[5] github.com/ypmen/TransientX
[6] psrchive.sourceforge.net
[7] dspsr.sourceforge.net
[8] epta.eu.org
[9] atnf.csiro.au
[10] github.com/danielemichilli/DM_phase
[11] github.com/CIRADA-Tools/RM-Tools
[12] gitlab.mpifr-bonn.mpg.de/nporayko/RMcalc

Table 1. Burst properties. *From left to right:* Burst number, barycentric arrival time in MJD, time in minutes since arrival time of burst 1, width, flux density, fluence, RM, circular polarization fraction, unbiased linear polarization fraction, drift rate, and PA (shifted by −90° to be distributed around zero). Uncertainties are 1σ. The listed PAs are the average PA of each burst weighted by their errors and the uncertainties are the standard deviation of the PA values. Burst 11 is considered a single event due to the baseline between the peaks being higher than the off-pulse baseline. However, due to the separation of the peaks we estimate a width, flux density, and fluence for each one.

Burst	MJD (59313+)	ΔT (min)	W (ms)	S (Jy)	F (Jy ms)	RM (rad m^{-2})	V/I (per cent)	$L_{\rm unb}/I$ (per cent)	D (MHz ms^{-1})	PA (°)
1	0.74325197	0	6.2 ± 0.5	0.17 ± 0.03	1.06	−608.5 ± 8.6	6 ± 7	56 ± 5	−41.7 ± 1.8	24 ± 9
2	0.74897156	8.24	19.3 ± 0.4	0.48 ± 0.07	9.27	−607.4 ± 0.6	−11 ± 1	92 ± 1	−19.4 ± 0.1	5 ± 6
3	0.75327832	14.44	15.5 ± 0.2	0.23 ± 0.03	3.54	−601.9 ± 0.4	−1 ± 1	94 ± 1	−34.9 ± 0.1	28 ± 4
4	0.76667874	33.73	9.0 ± 0.9	0.10 ± 0.02	0.92	−599.2 ± 4.4	3 ± 4	90 ± 5	−51.1 ± 2.1	24 ± 11
5	0.76668105	33.74	8.5 ± 0.3	0.50 ± 0.07	4.28	−620.4 ± 4.2	−20 ± 2	99 ± 2	−52.0 ± 0.4	−6 ± 5
6	0.77488410	45.55	22.2 ± 1.6	1.27 ± 0.19	28.12	−608.3 ± 0.3	6 ± 1[a]	98 ± 1	−16.5 ± 0.1	35 ± 2
7	0.78795702	64.38	5.6 ± 0.6	0.40 ± 0.06	2.22	−604.6 ± 2.5	3 ± 2	97 ± 2	−88.6 ± 0.6	41 ± 6
8	0.80949925	95.40	6.4 ± 0.5	0.16 ± 0.02	1.02	−612.0 ± 5.8	0 ± 4	90 ± 4	−51.4 ± 0.8	−6 ± 7
9	0.81914765	109.29	10.3 ± 0.3	2.31 ± 0.35	23.78	−584.1 ± 0.3	−5 ± 1	99 ± 1	−29.0 ± 0.1	10 ± 2
10	0.82721002	120.90	7.1 ± 1.1	0.09 ± 0.01	0.66	−604.7 ± 11.7	−3 ± 9	78 ± 8	−45.8 ± 2.8	−27 ± 11
11a	0.82721037	120.90	7.8 ± 0.8	0.06 ± 0.01	0.47	−601.2 ± 11.7	7 ± 4	84 ± 4	−108.3 ± 11.1	13 ± 11
11b			7.1 ± 1.0	0.07 ± 0.02	0.47					
12	0.83062730	125.82	11.1 ± 0.3	0.10 ± 0.01	1.09	−618.0 ± 1.4	−3 ± 1	90 ± 1	−28.5 ± 0.1	9 ± 6
13	0.83240637	128.38	12.1 ± 0.7	0.06 ± 0.01	0.76	−599.4 ± 2.7	10 ± 4	100 ± 3	−32.3 ± 0.5	−1 ± 8
14	0.84107824	140.87	9.7 ± 0.8	0.12 ± 0.02	1.19	−600.5 ± 6.3	3 ± 5	91 ± 4	−28.9 ± 0.3	−3 ± 10
15	0.84379515	144.78	4.8 ± 0.1	0.57 ± 0.09	2.75	−614.7 ± 1.3	−6 ± 2	100 ± 2	−65.2 ± 0.2	6 ± 4
16	0.84713858	149.60	10.4 ± 0.3	0.09 ± 0.01	0.94	−616.9 ± 1.3	4 ± 1	96 ± 2	−23.7 ± 0.1	6 ± 7
17	0.85342708	158.65	7.5 ± 1.5	0.12 ± 0.02	0.91	−601.8 ± 4.4	−3 ± 4	96 ± 4	−59.9 ± 1.2	−13 ± 7
18	0.85674812	163.43	7.4 ± 0.5	0.14 ± 0.02	1.02	−579.5 ± 6.7	−17 ± 5	84 ± 4	−46.0 ± 1.6	29 ± 6
19	0.88723065	207.33	4.7 ± 0.4	0.14 ± 0.02	0.63	−592.5 ± 5.0	0 ± 4	92 ± 4	−94.0 ± 5.7	−22 ± 6
20	0.89050534	212.04	5.9 ± 0.1	1.51 ± 0.23	8.94	−624.0 ± 0.6	−21 ± 1	96 ± 1	−45.9 ± 0.1	18 ± 3

Notes. [a]Absolute Stokes V values used.
Removing the baseline can result in $I \geq \sqrt{Q^2 + U^2 + V^2}$ not being fulfilled.

3.2 DM and RM

We estimate a singular DM that we apply to all our bursts. Using the results of `DM_phase` of the multicomponent bursts 2, 3, 6, 11, and 12, we obtain an average DM and error of 411.6 ± 0.6 pc cm^{-3}.

According to the NE2001 Galactic electron density model (Cordes & Lazio 2002), the Galactic DM contribution along the line of sight towards FRB 20201124A is 123 ± 25 pc cm^{-3} (20 per cent accuracy, e.g. Deller et al. 2009). For YMW16, the Galactic DM contribution is 197 pc cm^{-3} (Yao, Manchester & Wang 2019). We assume a DM of 50–80 pc cm^{-3} from the Galactic halo (Prochaska & Zheng 2019). The estimated redshift of the host galaxy of FRB 20201124A is 0.098 ± 0.002 (Kilpatrick et al. 2021), and the intergalactic medium (IGM)–redshift relation from Macquart et al. (2020) yields an IGM DM contribution of 82^{+17}_{-30} pc cm^{-3} (1σ). The resulting host galaxy DM is thus 140^{+33}_{-42} pc cm^{-3}.

The RMs we obtain for our bursts are listed in Table 1 and plotted over time in minutes with respect to the first burst in the upper panel of Fig. 2. We also plot the weighted mean RM value of −601 rad m^{-2}. The lower panel of Fig. 2 shows the FDF of our bursts. The standard deviation of the burst RMs is 11.1 rad m^{-2}, which is a fractional variation of 1.8 per cent from the mean.

From the coordinates of FRB 20201124A, we can calculate the Galactic RM contribution[13] based on the Galactic RM foreground map from Oppermann et al. (2015), and obtain a value of −57 ± 33 rad m^{-2}. We assume that the IGM has a negligible contribution to the RM (e.g. Oppermann et al. 2015). The majority of the measured RM must therefore originate from the host galaxy and local environment of FRB 20201124A that amounts to an observed RM of −548 ± 35 or −661 ± 42 rad m^{-2} in the redshifted source frame.

[13] github.com/FRBs/FRB

3.3 Polarimetry

All our bursts exhibit a high linear polarization fraction, consistent with linear polarization of other repeating FRBs (e.g. Michilli et al. 2018; Chawla et al. 2020; Hilmarsson et al. 2021; Nimmo et al. 2021a). For bursts 2, 5, 6, 9, 13, 18, and 20, we find evidence of circular polarization, ranging from absolute Stokes V/I fractions of 6–21 per cent. For the other bursts the circular polarization is consistent with noise, i.e. the Stokes V on/off-pulse standard deviation does not differ. Linear and circular polarization fractions are listed in Table 1. The measured linear polarization, $L = \sqrt{Q^2 + U^2}$, is overestimated in the presence of noise. We therefore use the unbiased linear polarization (Everett & Weisberg 2001)

$$L_{\rm unb} = \begin{cases} \sigma_I \sqrt{\left(\frac{L}{\sigma_I}\right)^2 - 1} & \text{if } \frac{L}{\sigma_I} \geq 1.57 \\ 0 & \text{otherwise,} \end{cases} \quad (1)$$

where σ_I is the Stokes I off-pulse standard deviation. Henceforth, all mention of linear polarization refers to $L_{\rm unb}$.

We split our band into four sub-bands to see if the circular polarization is localized to specific parts of the band. Most of the bursts do not cover the entire band, so both Stokes I and V are only seen in some of the sub-bands. However, burst 20 covers most of our band and has a relatively high circular polarization fraction that is consistent across all sub-bands.

The PAs are flat across the bursts, but show slight variations between bursts. The mean of the medians of the burst PAs is 8° with a standard deviation of 18°. Fig. 3 shows the PA over time of our bursts

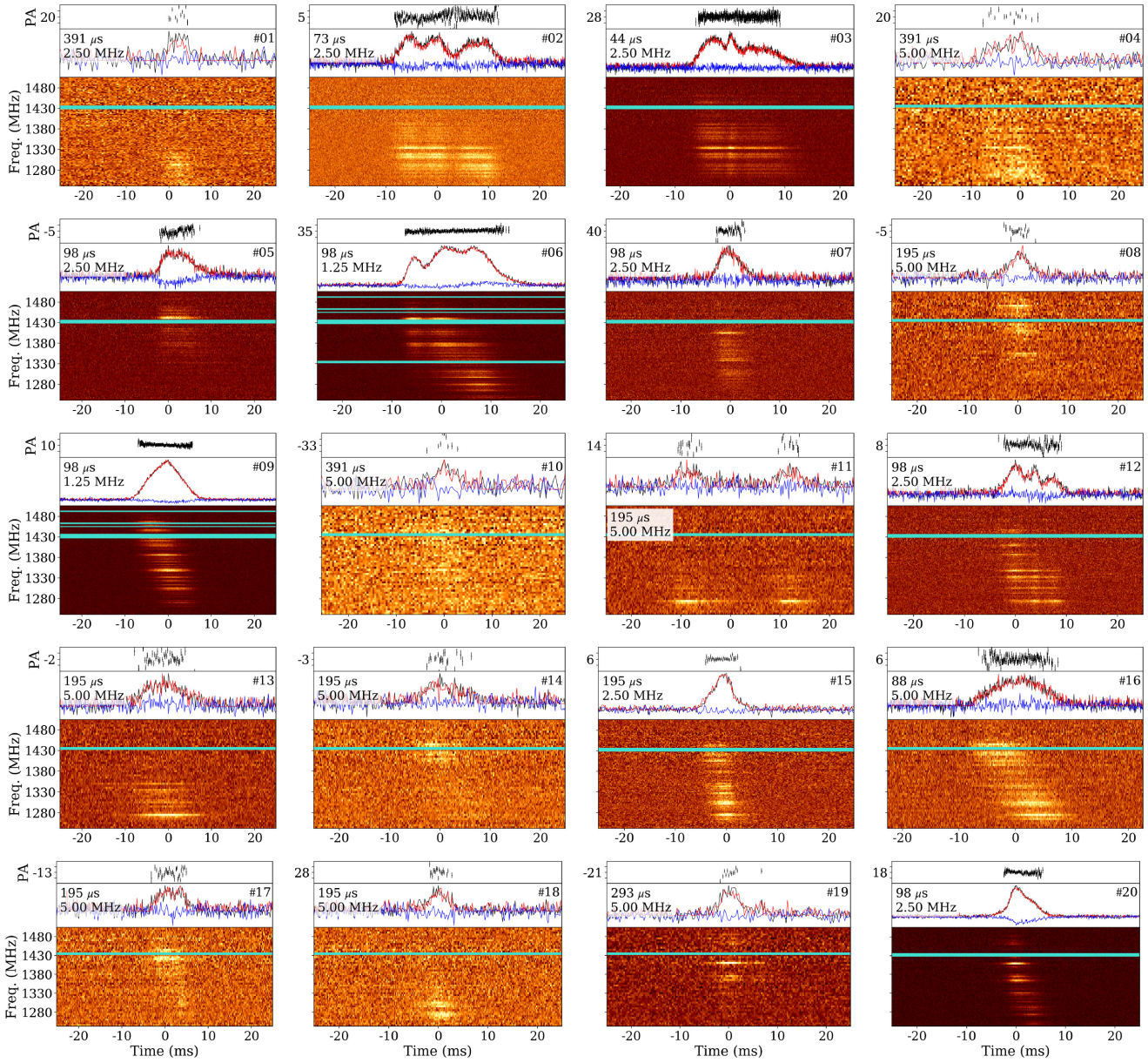

Figure 1. Dynamic spectra of the bursts. Turquoise horizontal strips are zapped channels. On top of each spectrum is the profile of the burst in total intensity (black), unbiased linear polarization (red), and circular polarization (blue), and the PA. The PA panel range is 40° around the median PA value (shifted by −90°) of each burst. The time and frequency resolution of each burst are written to the left of its profile, as they are downsampled and sub-banded to varying degrees for clarity. The burst number (as in Table 1) is to the right of each profile.

relative to their arrival time in minutes (top panel) and sequentially (bottom panel). If all the bursts are derotated to the average RM of −605 rad m^{-2}, we find the burst-to-burst PA variation slightly larger than when the bursts are derotated to their specific RM value. Our PAs are calculated with respect to a reference angle at infinite frequency (PA = RMλ^2 + PA$_\infty$).

3.4 Spectro-temporal properties

A downward drift in frequency can clearly be seen for many of our bursts in Fig. 1. We quantify the drifts using a 2D autocorrelation function. We perform a 2D autocorrelation of the intensity of each burst, using the same time and frequency ranges and resolutions as Fig. 1. We fit the result with a 2D rotated Gaussian, from which we obtain the burst drift rate; the results are listed in Table 1, and an example output of the drift analysis for burst 20 is shown in Fig. 4.

Our burst widths, with a mean value of 9.5 ms, are unusually large when compared to other repeating FRBs observed at 1.4 GHz (e.g. CHIME/FRB Collaboration 2019; Hessels et al. 2019; Fonseca et al. 2020). These widths are likely intrinsic to the burst, as scattering inferred from the scintillation bandwidth of these bursts is $\tau_{1\,\mathrm{GHz}} = 3.1 \pm 0.06$ µs (Main et al. 2021) and we do not observe a consistent asymmetry in the trailing edges of the burst profiles that would be consistent with scattering.

Burst 11 is considered a single burst here due to the fact that there are only a few milliseconds between its peaks and that the baseline between the peaks is higher than the off-pulse baseline. We still however split the burst into sub-bursts *a* and *b* with separate widths.

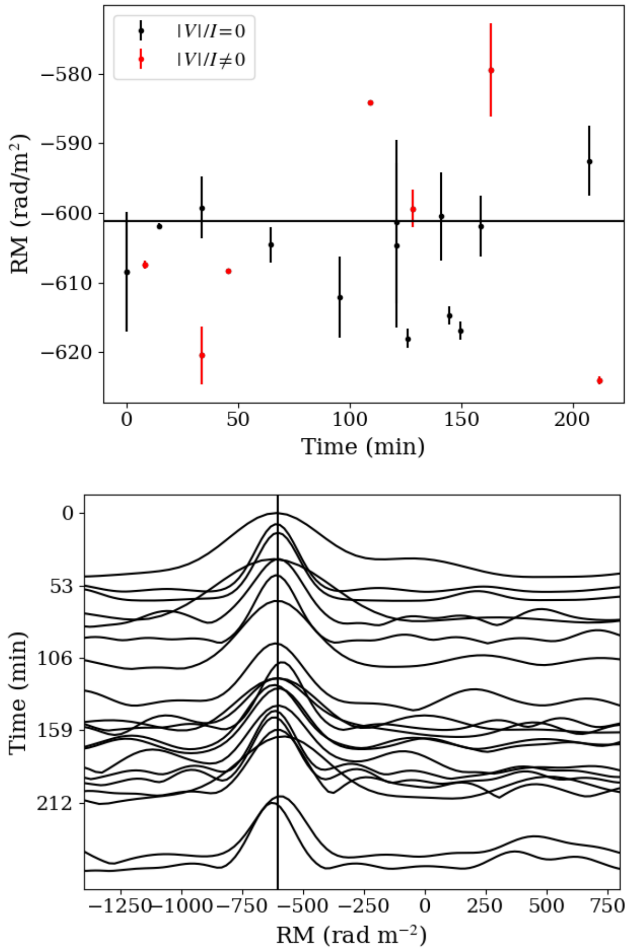

Figure 2. *Top*: RM over time of detected bursts. The horizontal line is the weighted mean RM of all the bursts, −601 rad m^{-2}. Black points are bursts with circular polarization fraction consistent with noise, red points are bursts with non-zero circular polarization fractions. *Bottom*: FDFs of the bursts, scaled to the same height. Peaks of the FDFs are at a time in minutes relative to the first burst as in Table 1. The vertical line shows the weighted mean RM value of the bursts.

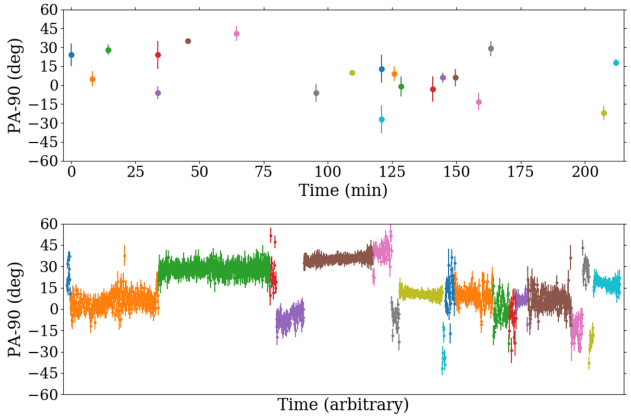

Figure 3. *Top:* Weighted average PA of each burst over time (shifted by −90°) as listed in Table 1. *Bottom:* PAs across each burst envelope as in Fig. 1 shown sequentially.

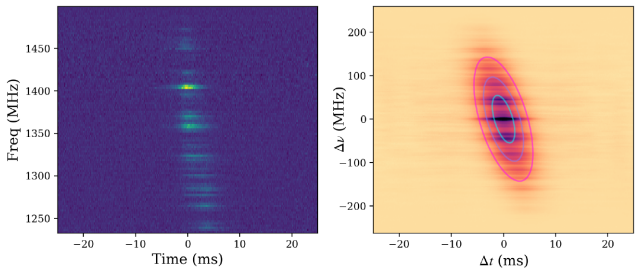

Figure 4. Drift analysis of burst 20. *Left:* Dynamic spectrum of the burst, dedispersed to 411.6 pc cm^{-3}, with the same time and frequency binning as in Fig. 1. *Right:* 2D ACF of the burst. Contours show the 1σ, 2σ, and 3σ widths of the best-fitting 2D Gaussian, used to derive the drift rate. The fine frequency structure arises from the scintillation, and is unrelated to the downward drift.

4 DISCUSSION

FRB 20201124A is the first repeating FRB to show clear signs of circular polarization, with circular polarization fractions up to 20 per cent in roughly one-third of the sample. We note that the bursts with non-zero circular polarization occur throughout the observation and never occur consecutively. This suggests the mechanism is time variable on short time-scales. There is no correlation between non-zero circular polarization and PAs, which one may expect if the bursts originate in a neutron star magnetosphere. In Fig. 2, one can see that four of the bursts with non-zero *V*/*I* have the four most extreme RM values (bursts 5, 9, 18, and 20).

The high linear polarization fractions, flat PAs across burst envelopes, and drift rates of FRB 20201124A are consistent with what has been observed in most other repeating FRBs including FRB 20121102A, FRB 20180916B, and FRB 20200120E (Michilli et al. 2018; Hessels et al. 2019; CHIME/FRB Collaboration 2020; Hilmarsson et al. 2021; Nimmo et al. 2021a, b). The exception is FRB 20180301A, which exhibits variable, linear polarization $<$ 100 per cent, and a drifting PA across the burst envelopes but no circular polarization (Luo et al. 2020). FRB 20201124A is, therefore, similar in many way to other repeating FRBs, but its non-zero circular polarization observable in some, but not all, makes the observed properties of repeaters even more diverse.

Comparisons are often made between FRBs and pulsar giant pulses (GPs), particularly those from the Crab pulsar. Hessels et al. (2019) noted the similarity in the banded structure observed in the spectra of Crab giant pulses detected at higher radio frequencies ($\gtrsim$5 GHz) from the interpulse (so-called HFIP GPs) and the band-limited emission in repeating FRBs. Jessner et al. (2010) measured the polarization properties of a large sample of giant pulses at 8.5 and 15.1 GHz from both the main pulse (MP) and interpulse (IP). A large fraction of the GPs from both the MP and IP have 100 per cent linear polarization, but pulses with circular polarization fractions between a few – of the order of 10 per cent were not uncommon. What is markedly different between the MP and IP GPs is the variation in PA. While PAs for the MPs were varied between 0 and 180°, the PAs for IPs were more restricted in range with $\sim$ 80 per cent of the bursts having PAs that varied within 30° (Jessner et al. 2010). Fig. 3 shows that the variation in the PAs from FRB 20201124A is similar, with most PAs falling within a 30–40° range. Combined with the banded structure seen in the dynamic spectra, bursts from FRB 20201124A show striking similarities to the HFIP GPs from the Crab pulsar.

Polarization observations of the magnetar XTE J1810−197 (Kramer et al. 2007) also show noticeable similarities to

FRB 20201124A. The profiles of XTE J1810−197, both single pulse and averaged over multiple epochs, have high degrees of linear polarization and low but significant degree of circular polarization. The PAs are also slightly slanted across the profile, which is more akin to what we see from FRB 20201124A and other repeating FRBs rather than the S-like swing seen from pulsars.

In magneto-active plasma, linearly polarized radiation can be converted into circular in a process called 'Faraday conversion' or 'generalized Faraday rotation'. Vedantham & Ravi (2019) and Gruzinov & Levin (2019) have discussed this effect on FRB 20121102A for relativistic and non-relativistic cases, respectively. However, it is challeging for this effect to account for the change of circular polarization of FRB 20201124A. First, the change of RM is only $\sim$10 rad m^{-2} for the bursts with circular polarization. Given a host DM of $\sim$100 pc cm^{-3}, it corresponds to magnetic field strength of only μG with the cyclotron frequency $f_B = 2.8\,\mathrm{MHz\,G^{-1}}\,B$ $\sim$Hz. In this case, f_B is nine orders of magnitude lower than the observation frequency at GHz, while Faraday conversion usually happens when the cyclotron frequency is approaching the observation frequency. Even if only a small fraction of DM is contributing to the RM, and the B field is several orders larger, it is difficult to bridge the difference of nine orders of magnitude, otherwise the local electron density would be too low and the electric field would again not experience the Faraday conversion. Secondly, bursts separated by minutes are seen to have different circular fractions, which gives an estimate of the spatial scale of changes assuming the typical velocity of few hundred km s^{-1} for neutron stars. This rules out the scenario of Faraday conversion with weak magnetic field, where the EM wave adiabatically tracks a slow field reversal in the LOS (Gruzinov & Levin 2019). On the other hand, if there is a group of highly relativistic electrons introducing the Faraday conversion, the circular and linear rotation can be modelled with RRMλ^3 (Kennett & Melrose 1998). The limited bandwidth has prevented us from distinguishing λ^2 rotation from RM and λ^3 rotation from RRM and hence the observed RM variation could be due to RRM, which will introduce various levels of circular polarization depending on the local magnetic field, electron density, and the angle between field line and polarization angle. However, assuming the field to be fully linearly polarized at infinite frequency, given the observed low circular fraction, any Faraday conversion has to be incomplete. Therefore, the fraction in the lower band would be higher than that in the upper band. With λ^3 dependence, the polarization fraction at the bottom of the band should be $\sim$1.5 times the polarization fraction at the top of the band, which is not seen in the data. Therefore, we conclude that the observed circular polarization may be intrinsic to the source.

In terms of RM magnitude among repeating FRBs, FRB 20201124A is similar to FRB 20190303A and FRB 20180301A (Fonseca et al. 2020; Luo et al. 2020), while others seem to be more or less consistent with the Galactic RM contribution (FRB 20180916B, FRB 20190604A, FRB 20200120E; CHIME/FRB Collaboration 2019; Fonseca et al. 2020; Nimmo et al. 2021b). Finally, there is FRB 20121102A with its enormous RM of $\sim10^5$ rad m^{-2} (Michilli et al. 2018; Hilmarsson et al. 2021).

Similar temporal RM variability is seen in FRB 20180301A (Luo et al. 2020) where its RM varies between 520 and 560 rad m^{-2} over a 1-d time-scale and is thought unlikely to be a constant. Another example is the RM variation of FRB 20121102A, showing RM differences of $\sim10^2$ rad m^{-2} over 1-h time-scales (Michilli et al. 2018). However, in that case a global RM average is calculated for each observing epoch. In this context, FRB 20180916B has no short time-scale measurements but has been observed to be consistent with its original RM value of −115 rad m^{-2} (Nimmo et al. 2021a) and seen to decrease by only a few rad m^{-2} over the course of a year (Pleunis et al. 2021). Further polarization measurements of FRB 20201124A will determine the stability of its RM.

Assuming that all the host DM is contained within the Faraday rotating medium, we can estimate a source frame average magnetic field strength along the line of sight as

$$\langle B_\parallel \rangle = 1.23\,\mathrm{RM_{src}/DM_{host}}\ \mu\mathrm{G} \quad (2)$$

and obtain an estimate of 4–6 μG. If the RM originates in a small physical region close to the source, such as the remnants of a supernova, the amount of DM in this Faraday rotating medium could be much smaller, and the above estimate is a lower limit.

RM variations on a time-scale of minutes must arise from spatial variations in the electron density and/or LoS magnetic field strength close to the source. The observed fractional RM variations are roughly 2 per cent. Assuming a constant DM, the magnetic field strength variations must be of the order of 0.1 μG. If instead the observed RM variation is due to changes in the host DM contribution, the host DM must vary by 2–4 pc cm^{-3}, which translates to a fractional variation of the total observed DM of 0.7 per cent. This change is inconsistent with our lack of change in DM between bursts, suggesting that either the RM variations are due to small-scale magnetic field variations or only a fraction of the estimated host DM contributes to the RM.

We also note that the RM measurement uncertainties of FRB 20201124A could also be underestimated and the RM value is, in fact, constant with time. The FDFs in the lower panel of Fig. 2 show that the mean RM is well contained within their widths.

We can consider the model of a magnetar within a supernova remnant from Margalit & Metzger (2018), where bursts are generated by a synchrotron maser due to shocks from the magnetized outflow of the magnetar into its circumsource material. The RM generating material is contained within the expanding magnetar nebula, and for our mean RM magnitude of 601 rad m^{-2} we obtain source ages between 60 and 200 yr. At this age, the coincident, compact PRS should be at the μJy level, which is consistent with the non-detection of such a source associated with FRB 20201124A (Marcote et al. 2021; Ravi et al. 2021). Within this framework, the source ages of FRB 20121102A and FRB 20180916B have been estimated to be $\sim$10 and $\sim$300 yr, respectively (Marcote et al. 2020; Hilmarsson et al. 2021).

Prior to being found to be periodic in its activity, bursts from FRB 20121102A appeared to follow a Weibull distribution, i.e. clustered in time with a Weibull clustering factor of $k = 0.34$ (Oppermann, Yu & Pen 2018). Within a typical observation time of a few hours, bursts from FRB 20121102A follow a Poissonian distribution (Cruces et al. 2021). If FRB 20201124A is periodic in its activity, one can expect burst arrival times to follow a Weibull distribution over long time-scales until a periodicity is found.

As mentioned in Section 3, the mean and narrowest burst durations of our sample are 9.5 and 4.7 ms, respectively. By comparison, the peak of the width distribution of $\sim$1600 bursts from FRB 20121102A is $\sim$4 ms (Li et al. 2021). The widths of four bursts detected from FRB 20200120E range from 50 to 150 μs (Nimmo et al. 2021b). Therefore, the characteristic burst duration varies over two orders of magnitude among the known repeating FRBs. If bursts from repeating FRBs originate in the magnetosphere of neutron stars, the characteristic duration may correlate with rotational period, as seen in micro-structure of pulsar single pulses (e.g. Kramer, Johnston & van Straten 2002).

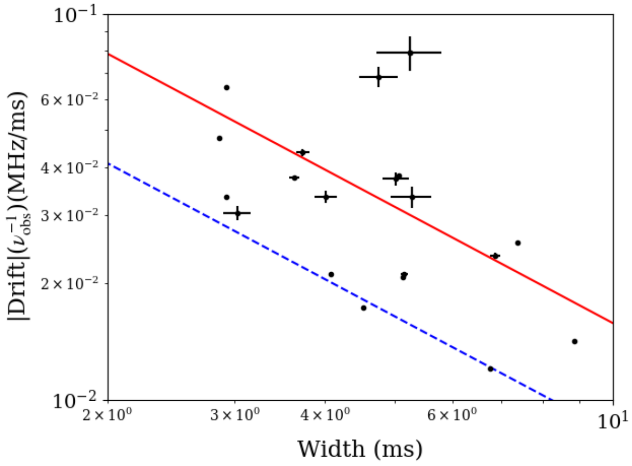

Figure 5. Best-fitting 2D Gaussian widths versus absolute burst drifts scaled by the central observing frequency. Red line shows the best fit through the data and the blue dashed line shows the results from Chamma et al. (2021).

Chamma et al. (2021) investigate the relation between burst widths and drift rates within the framework of Dicke's superradiance, and find a linear relation between the two. We plot the burst widths versus drift for our burst sample in Fig. 5. To be consistent with the methods in Chamma et al. (2021), we use the 1σ widths of the fitted rotated 2D Gaussians (right-hand panel in Fig. 4) projected on to the time axis. A best-fitting line through our data points yields a similar slope to the results of Chamma et al. (2021), but slightly offset towards higher widths.

5 SUMMARY

We have detected 20 bursts from FRB 20201124A from a single 4-h observation on 2021 April 9 with the Effelsberg 100-m radio telescope at 1.4 GHz. As commonly seen in repeating FRBs, FRB 20201124A exhibits a downward drift in frequency over time in many of its bursts. However, the burst widths are wider than normally seen at this frequency, with a mean value of 9.5 ms. The bursts in our sample are highly linearly polarized ($\gtrsim$ 75 per cent), with a sub-set of them also being circularly polarized ($\lesssim$ 20 per cent), which is the first for a repeating FRB. We obtain an average DM of 411.6 ± 0.6 pc cm^{-3}. The RM of FRB 20201124A varies slightly between bursts around their weighted mean of -601 rad m^{-2}. Interestingly, the bursts with circular polarization have the most extreme RM values in our sample. We hope that future polarization measurements of FRB 20201124A will help determine its RM stability.

ACKNOWLEDGEMENTS

This work is based on observations with the 100-m telescope of the MPIfR (Max-Planck-Institut für Radioastronomie) at Effelsberg. Part of this research has made use of the European Pulsar Network (EPN) Database of Pulsar Profiles maintained by the University of Manchester, which is available at jodrellbank.manchester.ac.uk/research/pulsar/Resources/epn/. GHH thanks Dr A. D. Seymour for insights into `DM_phase`, Dr N. K. Porayko for help with RM search methods and archive handling, and Dr M. Cruces for providing helpful code snippets. LGS is a Lise Meitner Max Planck independent research group leader and acknowledges funding from the Max Planck Society. We thank the anonymous referee for their helpful comments.

DATA AVAILABILITY

The data underlying this article will be shared on reasonable request to the corresponding authors.

REFERENCES

Barr E. D. et al., 2013, MNRAS, 435, 2234
Brentjens M. A., de Bruyn A. G., 2005, A&A, 441, 1217
Burn B. J., 1966, MNRAS, 133, 67
Chamma M. A., Rajabi F., Wyenberg C. M., Mathews A., Houde M., 2021, MNRAS, 507, 246
Chawla P. et al., 2020, ApJ, 896, L41
CHIME/FRB Collaboration, 2019, ApJ, 885, L24
CHIME/FRB Collaboration, 2020, Nature, 582, 351
CHIME/FRB Collaboration, 2021a, Astron. Telegram, 14497, 1
CHIME/FRB Collaboration, 2021b, ApJS, preprint (arXiv:2106.04352)
Cordes J. M., Lazio T. J. W., 2002, preprint (arXiv:astro-ph/0207156)
Cruces M. et al., 2021, MNRAS, 500, 448
Day C. K., Bhandari S., Deller A. T., Shannon R. M., Moss V. A., 2021, Astron. Telegram, 14515, 1
Deller A. T., Tingay S. J., Bailes M., Reynolds J. E., 2009, ApJ, 701, 1243
Everett J. E., Weisberg J. M., 2001, ApJ, 553, 341
Fong W.-f. et al., 2021, ApJ, 919, L23
Fonseca E. et al., 2020, ApJ, 891, L6
Gruzinov A., Levin Y., 2019, ApJ, 876, 74
Hessels J. W. T. et al., 2019, ApJ, 876, L23
Hilmarsson G. H. et al., 2021, ApJ, 908, L10
Hotan A. W., van Straten W., Manchester R. N., 2004, Publ. Astron. Soc. Aust., 21, 302
Jessner A. et al., 2010, A&A, 524, A60
Kennett M., Melrose D., 1998, PASA, 15, 211
Kilpatrick C. D., Fong W., Prochaska J. X., Tejos N., Bhandari S., Day C. K., 2021, Astron. Telegram, 14516, 1
Kramer M., Johnston S., van Straten W., 2002, MNRAS, 334, 523
Kramer M., Stappers B. W., Jessner A., Lyne A. G., Jordan C. A., 2007, MNRAS, 377, 107
Law C., Tendulkar S., Clarke T., Aggarwal K., Bethapudy S., 2021, Astron. Telegram, 14526, 1
Li D. et al., 2021, Nature, 598, 267
Luo R. et al., 2020, Nature, 586, 693
Macquart J. P. et al., 2020, Nature, 581, 391
Main R. A., Hilmarsson G. H., Marthi V. R., Spitler L. G., Wharton R. S., Bethapudi S., Li D. Z., Lin H. H., 2021, MNRAS, preprint (arXiv:2108.00052)
Manchester R. N., Hobbs G. B., Teoh A., Hobbs M., 2005, AJ, 129, 1993
Marcote B. et al., 2020, Nature, 577, 190
Marcote B. et al., 2021, Astron. Telegram, 14603, 1
Margalit B., Metzger B. D., 2018, ApJ, 868, L4
Michilli D. et al., 2018, Nature, 553, 182
Nimmo K. et al., 2021a, Nat. Astron., 5, 594
Nimmo K. et al., 2021b, preprint (arXiv:2105.11446)
Oppermann N. et al., 2015, A&A, 575, A118
Oppermann N., Yu H.-R., Pen U.-L., 2018, MNRAS, 475, 5109
Pastor-Marazuela I. et al., 2020, preprint (arXiv:2012.08348)
Pearlman A. B., Majid W. A., Prince T. A., Bansal K., Naudet C. J., Kocz J., 2021, Astron. Telegram, 14519, 1
Pleunis Z. et al., 2021, ApJ, 911, L3
Porayko N. K. et al., 2019, MNRAS, 483, 4100
Prochaska J. X., Zheng Y., 2019, MNRAS, 485, 648
Purcell C. R., Van Eck C. L., West J., Sun X. H., Gaensler B. M., 2020, Astrophysics Source Code Library, record ascl:2005.003

Rajwade K. M. et al., 2020, MNRAS, 495, 3551
Ransom S., 2011, Astrophysics Source Code Library, record ascl:1107.017
Ravi V. et al., 2021, MNRAS, preprint (arXiv:2106.09710)
Ricci R., Piro L., Panessa F., O'Connor B., Lotti S., Bruni G., Zhang B., 2021, Astron. Telegram, 14549, 1
Seymour A., Michilli D., Pleunis Z., 2019, Astrophysics Source Code Library, record ascl:1910.004
Spitler L., Hilmarsson H., 2021, Astron. Telegram, 14537, 1
Spitler L. G. et al., 2016, Nature, 531, 202
van Straten W., Bailes M., 2011, Publ. Astron. Soc. Aust., 28, 1
Vedantham H. K., Ravi V., 2019, MNRAS, 485, L78
Wharton R. et al., 2021a, Astron. Telegram, 14529, 1
Wharton R. et al., 2021b, Astron. Telegram, 14538, 1
Yao J., Manchester R. N., Wang N., 2019, Astrophysics Source Code Library, record ascl:1908.022

This paper has been typeset from a TEX/LATEX file prepared by the author.